



N64-24989

CODE-1

047.05

# MICROMETEORITE IMPACT STUDIES

by

J. C. SLATTERY

prepared for

NATIONAL AERONAUTICS AND SPACE ADMINISTRATION

OTS PRICE

XEROX

\$

5.60 ph

MICROFILM

\$

**TRW** SPACE TECHNOLOGY LABORATORIES

THOMPSON RAMP WOOLBRIDGE INC

**FINAL REPORT**

**MICROMETEORITE IMPACT STUDIES**

by

**J. C. Slattery**

prepared for

**NATIONAL AERONAUTICS AND SPACE ADMINISTRATION**

**June 30, 1964**

**CONTRACT NAS 3-3569**

**Technical Management  
NASA Lewis Research Center  
Cleveland, Ohio  
Spacecraft Technology Division**

**PHYSICAL ELECTRONICS LABORATORY  
Physical Research Division  
TRW Space Technology Laboratories  
One Space Park  
Redondo Beach, California**

## MICROMETEORITE IMPACT STUDIES

by

J. C. Slattery

## ABSTRACT

A

24987

The burst of free charge produced by a hypervelocity particle impact was investigated. The hypervelocity particles were iron spheres with diameters ranging from 0.1 micron to 1.0 micron. The amount of charge produced per unit impacting particle mass was measured for several target materials at velocities from 3 km/sec to 25 km/sec. The effect was found to be independent of target temperature to 600°C, electric field to  $10^6$  volts/meter and small amounts of cesium contamination. Self-sustaining electrical discharges have been initiated in simulated ion engines by hypervelocity particle impacts.

*Slattery*  
*24987*

## TABLE OF CONTENTS

	Page
FIGURE CAPTIONS. . . . .	11
SUMMARY. . . . .	v
INTRODUCTION . . . . .	1
I.    Experimental Methods . . . . .	1
Data on Clean Metals. . . . .	3
Interpretation of Data. . . . .	4
Effect of Collecting Field. . . . .	6
Charge Emission for Cesium Covered Surfaces. . . . .	6
Summary . . . . .	7
II.   Discharges in Ion Engines. . . . .	7
Summary . . . . .	11
REPORT DISTRIBUTION LIST FOR CONTRACT No. NAS3-3369. .	27

## FIGURE CAPTIONS

## Page

1. Data illustrating the equality of positive and negative charge emission. The target was tungsten. The emitted charge, normalized to the mass of the impacting particle, is plotted as a function of particle velocity. The particles were iron spheres, ranging in diameter from 0.1 micron to 1.0 micron. . . . . 12
2. Charge emission from a tungsten target. Emitted charge, normalized to the impacting particle mass, is plotted against the particle velocity. The particles were iron spheres, ranging in diameter from 0.1 micron to 1.0 micron. . . . . 13
3. Charge emission from a tantalum target. Emitted charge, normalized to the impacting particle mass, is plotted against the particle velocity. The particles were iron spheres, ranging in diameter from 0.1 micron to 1.0 micron. . . . . 14
4. Charge emission from a molybdenum target. Emitted charge, normalized to the impacting particle mass, is plotted against the particle velocity. The particles were iron spheres, ranging in diameter from 0.1 micron to 1.0 micron. . . . . 15
5. Charge emission from a copper target. Emitted charge, normalized to the impacting particle mass, is plotted against the particle velocity. The particles were iron spheres, ranging in diameter from 0.1 micron to 1.0 micron. . . . . 16
6. Charge emission from a stainless steel target. Emitted charge, normalized to the impacting particle mass, is plotted against the particle velocity. The particles were iron spheres, ranging in diameter from 0.1 micron to 1.0 micron. . . . . 17
7. Charge collection from a tungsten target at target temperatures of 25°C and 600°C. The ordinate is emitted charge normalized to the impacting particle mass and the abscissa is particle velocity. The particles were iron spheres, ranging in diameter from 0.1 micron to 1.0 micron . . . . . 18

## FIGURE CAPTIONS CONTINUED

	Page
8. Effect of electric field on charge emission from a tantalum target. The emitted charge, normalized to the impacting particle mass, is plotted against particle velocity. The particles were iron spheres, ranging in diameter from 0.1 micron to 1.0 micron . . . . .	19
9. Charge emission from a molybdenum target showing the effect of a thin cesium film on target surface. The emitted charge, normalized to the impacting particle mass, is plotted against particle velocity. The particles were iron spheres, ranging in diameter from 0.1 micron to 1.0 micron. The estimated Cs coverage was a layer 0.1 micron thick. . . . .	20
10. Charge emission from a stainless steel target showing the effect of a thin cesium film on target surface. The emitted charge, normalized to the impacting particle mass, is plotted against particle velocity. The particles were iron spheres, ranging in diameter from 0.1 micron to 1.0 micron. The estimated Cs coverage was a layer 0.1 micron thick. . . . .	21
11. Oscilloscope tracings illustrating a particle which does not cause a discharge (11-a) and one which does (11-b). In both figures the top trace is of the particle detector, vertical sensitivity 0.2 v/div and sweep speed 10 $\mu$ sec/div. The bottom trace is from a high voltage probe connected to the grid in front of the target, vertical sensitivity 2000 volts/div and sweep speed 10 $\mu$ sec/div . . . . .	22
12. Behavior of the high voltage on the grid during discharge with three different capacitors in parallel with the grid. Vertical scale is 2000 volts/div, sweep speed is 0.2 $\mu$ sec/div. Capacitances are: (12-a) C = 3 $\mu$ f, (12-b) C = 500 $\mu$ f, (12-c) C = 0.06 $\mu$ f . . . . .	23
13. Polaroid pictures of particle initiated discharges. Figure 13-a shows the field of view, with a particle detector on the right, the grid just to the left of the particle detector and then the target to the left of the grid. The target appears as a thin line in the photograph. Figures 13-b and 13-d are with a positive voltage applied to the grid and 13-c and 13-e with a negative voltage. See text for a fuller discussion . . . . .	24

## FIGURE CAPTIONS CONTINUED

	Page
14. Fast-camera framing pictures of particle initiated discharges. The oscilloscope tracings show the time relationship between the three exposures (top trace) and the discharging high voltage on the grid (bottom trace). The sweep speeds were both $0.5 \mu\text{sec}/\text{div}$ . Two separate discharges are shown in the photograph and the exposure on the right is the first in both cases. . . . .	25
15. Fast-camera streak pictures of particle initiated discharges. The oscilloscope tracings show the time relationship between the streak time (top trace) and the discharging high voltage on the grid (bottom trace). The oscilloscope sweep speeds are both $0.5 \mu\text{sec}/\text{div}$ . There was no slit in the system and the entire image (as shown in Fig. 14) is being swept across the film. Two discharges are shown and in both cases the sweep starts at the right and moves to the left. . . . .	26

## MICROMETEORITE IMPACT STUDIES

by J. C. Slattery

TRW Space Technology Laboratories

### SUMMARY

An investigation was made of the mechanism of charge production by hypervelocity impact. This effect is related to the risk of micrometeoroid damage to ion engines operating in outer space. It was found that the impact of a small (micron-sized) hypervelocity particle produces a burst of free charge; positive and negative in equal amounts. The charge production per unit particle mass was measured over a velocity range of 3 km/sec to 25 km/sec for five target materials: tungsten, tantalum, molybdenum, copper and stainless steel. The impacting particles were iron spheres with diameters in the 0.1-micron to 1.0-micron range. Charge production was found to be independent of target temperature to 600°C, electric field at the target surface to  $10^6$  volts/meter, and small amounts of cesium contamination on the target surface. A plausible model of the charge production mechanism was developed. Simulated ion engines were also bombarded. A substantial fraction of the impacts (approximately 5%) produced self-sustaining electrical discharges in the simulated ion engines.

## INTRODUCTION

Some time ago, it was discovered at TRW Space Technology Laboratories that the impact of a simulated micrometeorite into a solid target produces a relatively large burst of free charge\*. There is no reason to suspect that natural meteorites will not exhibit the same behavior. With this in mind a program under NASA Contract No. NAS3-3569 was undertaken to examine the phenomenon and its possible effect on ion engines. The work under this contract divided logically into two categories: (1) the amount of charge produced by a micrometeorite impact and (2) whether or not this charge could initiate a self-sustaining discharge under conditions approximating an operating ion engine. These two categories are discussed separately below, although the first has obvious bearing on the second.

### I. EXPERIMENTAL METHODS

There are several features common to all the experiments described in this report. The hypervelocity particles are generated by the STL two-million-volt Van de Graaff generator. A contact charging method puts a high charge on micron sized iron grains which are then accelerated through the Van de Graaff voltage. Before reaching the experiment the particles pass through one or more particle detectors, usually cylindrical in shape. They are observed by the voltage signal which they induce on the capacitance of the detector.

The charge on each particle is deduced from the known detector capacitance and the magnitude of the induced voltage. The particle velocity is derived from the transit time through the detector. Knowing the particle charge, the accelerating voltage and the velocity, the particle mass may be calculated. The detector signal from every particle in an experiment is photographed and the mass and velocity of each particle are calculated.

The experiments on charge production all used a target and grid arrangement to observe the charge produced. The parallel target and grid were positioned normal to the incoming particle trajectory, and were separated by one to ten millimeters. A bias voltage was always present between target and grid. The impacting particle passed through the

---

\*"Ionization Associated with Hypervelocity Impact," J. F. Friichtenicht and J. C. Slattery, NASA TN D-2091.

grid and struck the target. Any charge created by the impact was drawn off by the applied bias voltage and, depending on the polarity of this voltage, either positive or negative charge carriers would leave the target.

Since the incoming particle was always charged, and this charge was deposited on the target, it was necessary to correct for this effect. This was done in every case. Usually, the amount of charge created in the impact was much greater than that brought in by the particle.

While performing the first experiments it became apparent that the charge produced by an impact could be divided into two parts: a primary charge production by the initial impact, and a secondary charge production by "spray particles". This term is used to refer to the matter which is ejected in varying amounts from the site of an impact. It apparently comes off, partly as large particles, and partly as a metallic vapor. It is observed that when ejected matter strikes the grid or grid supports, it makes more charge which is drawn into the target.

Since the velocity and size distribution of the spray particles is not known, initial experiments concentrated on the primary particles. This was done by placing high transmission grids in front of the target in order to minimize the interception of spray particles ejected from the target, together with discrimination by time-of-flight methods in the measurement circuit. The ions or electrons produced by the original impact are collected in a very short time, while the time required for a spray particle to travel from the target to wherever it finally impacts, is much longer (3 or 4 microseconds).

For absolute measurement of charge production, the method used was to integrate the charge on a small capacitance (either the target or grid) and to observe the voltage change on this capacitance with a high impedance amplifier. Care must be taken not to include charge produced by spray particles. This is accomplished by a careful choice of the RC-decay time of the collecting capacitance relative to the delay time between the arrival of the secondary charge produced by spray particles. In practice, a small amount of the original charge inevitably leaks off the capacitor before the secondary charge arrives. The voltage wave form produced in this manner rises sharply, then decays slightly for three or four microseconds, then rises again in steps to a value indicative of the burst from the spray. The first step is due to

charge produced by the original impact. One result learned from a considerable number of experiments of this type is that charge production is independent of the electric field at the target surface and of polarity of the charge being collected. If the applied voltage is high enough, this burst of charge will sometimes produce an electrical discharge.

Relative charge production measurements were made with collected capacitance shorted by a low impedance amplifier, giving a short time constant. This served to differentiate the signal more sharply and more fully to distinguish between initial charge and secondary charge from the spray particles. The voltage wave form produced by this method consists of a short spike, a delay, and then several more spikes. The first spike is the contribution of charge produced by the original impact, and the others are due to spray particles.

As long as the charge collection time is less than the amplifier rise time, there is a linear relationship between the height of the first spike and the amount of charge produced. In this manner one can compare relative charge production at different temperatures, or at different electric fields.

#### DATA ON CLEAN METALS

Data on charge emission have been collected for three different refractory materials: tungsten, tantalum and molybdenum; and for two constructor materials: copper and stainless steel. The charge emission has been examined, also, with different electric fields at the target surface, with different target temperatures (up to 600°C) and with a cesium contamination on the target. The particles were small iron spheres, with diameters in the 0.1 to 2.0 micron range. In the presentation of these data, the polarity of the charge emitted is not specified because the effects are independent of charge polarity. An impact produces the same number of ions and electrons and either species can be drawn off by an appropriate electric field. A number of experiments confirmed this point, and the data from one of these are illustrated in Fig. 1. The target in this case was tungsten and, as usual, the collected charge normalized to the mass of the impacting particle was plotted as a function of particle velocity.

This particular set of data was taken before our improved particle detectors were in use and extends to 6 km/sec.

However, later experiments show that the equality of positive and negative charge emission extends to at least 20 km/sec.

Figures 2, 3 and 4 illustrate the charge emission from the refractory metals: tungsten, tantalum and molybdenum, respectively. Again the ordinate shows charge emitted normalized to the impacting particle mass, plotted against particle velocity. The data on constructor materials, copper and stainless steel, are illustrated in Figs. 5 and 6, respectively.

The observed results indicate that the charge emission from copper is a factor of ten lower than for the other four materials. The refractory metals and stainless steel all have about the same charge emission. The reason for this material dependence is not completely understood, but it has been noticed before that materials considered "soft" will yield less charge than materials considered "hard". This point is discussed more fully below.

#### INTERPRETATION OF DATA

In all of these measurements, the total charge emitted is observed experimentally; not the current it produces as it flows between target and grid. The distance between target and grid (typically, 2 to 5 mm) and the applied voltage were such that the amplifiers could not observe the transit time of either electrons or ions. Thus, it was not possible to observe any time structure in the charge production process. It can be stated that the charge is produced in a time less than one-half microsecond.

This is a point which has bearing on the mechanism of the charge production. The mechanism is still not clear, but a model which fits the observed facts has been evolved.

It is difficult to reconcile the equality of the positive and negative charge collected with any type of current emission phenomenon. If it were not for this point, one could argue that the charge was being emitted from a small "hot spot" which existed for a fraction of a microsecond at the impact site. But ion current sources, at a given temperature and extraction voltage, will give a lower current than electron sources. This is true, not only because of the increased mass of the charge carrier in ion emission, but also, because the ion work functions are generally higher. Thus one would expect

orders of magnitude less ion current emission than electron current emission. Furthermore, the emission current should be sensitive to the applied electric field. Since no such difference is observed, one is led to the conclusion that ions and electrons are created in equal numbers and that the applied field serves merely to separate them, not entering into the creation process.

This suggests that the charge is present in the form of a dilute plasma. One way in which such a plasma could be formed is to concentrate the incoming particle energy into a small volume. The total energy carried by the particle is small, because the mass is small, however, the energy per atom in the particle is quite high. For example, a 6 km/sec particle has a kinetic energy per atom of about ten electron volts and, of course, this energy increases as the square of the velocity. When the particle impacts on a solid target this kinetic energy is transformed into other forms: shock waves, heat of melting and vaporization, and raising the temperature of the material.

If the original 10 ev/atom is spread over ten times as many atoms as a result of the impact, the resulting average energy corresponds to a temperature of 8000°K. (Assuming a monatomic gas with an atomic specific heat of  $3/2$  kT.) A small ball of gas at this temperature would have considerable ionization (several percent) associated with it. The little ball of gas and charge created by the impact is then driven outward from the target, expanding because of the high pressures at these high temperatures.

As the plasma continues to expand, it finally reaches a point where it is so dilute that the electric field can penetrate it and extract charge. At this point essentially all the charge of one polarity is extracted by the field, while the opposite polarity charge returns to the target. With this model in mind, one may predict the effect of electric field, target temperature and cesium contamination.

The target temperature should have very little effect, at least up to the melting point of the target. The extra energy due to the target temperature is still small compared to the energy per unit atom which has been hypothesized. This may not be true if the target temperature is so high that the atomic bonds are affected, that is, if the target is near melting. In that case the target would behave like a "soft" material and the particle energy could not be concentrated into a small volume. Figure 7 illustrates the data

from one of the experiments made to measure charge collection at room temperature and at 600°C. The target in this case was tungsten and very little temperature effect can be seen. The same experiment has been performed in our laboratory on the other two refractory metals, and also on copper and stainless steel, with the same results. These experiments have confirmed that although there is some spread in the data, no consistent temperature effect is present at temperatures up to 600°C.

### EFFECT OF COLLECTING FIELD

The magnitude of the electric field, which is applied to draw out the charge, should also have no effect, provided the field is high enough to overcome space charge and to separate the charge in the plasma before it makes contact with other electrodes in the system, and below the value at which substantial field emission takes place.

This has been checked experimentally on several materials, using fields which varied from  $4 \times 10^3$  volts/meter up to  $10^6$  volts/meter, with total voltages from 100 volts to 3000 volts. The results of one of these experiments are shown in Fig. 8. The charge collected from a tantalum target is plotted for two collecting fields,  $3.9 \times 10^4$  volts/meter and  $10^6$  volts/meter. There is no noticeable field effect, nor was there on any of the other materials tested. The applied voltages were low enough that no discharges occurred. The effect of applied voltage is discussed further in the second section of this report.

### CHARGE EMISSION FOR CESIUM COVERED SURFACES

The experiments performed to measure the cesium effect use a gun which evaporated cesium from a 0.010" hole onto the target at a low rate. The evaporation rate from the gun was such that it took about an hour to form a thin film exhibiting interference effects on a transparent cover plate located 3" away from the gun. The cesium beam impinged on the target at an angle of 83° from the vertical. The gun was located about 1" from the target. The procedure followed was to measure the charge yield from a target before turning on the cesium. The cesium was then turned on and sprayed at the target until a visible film formed, and then the charge yield was remeasured. Some of these data are illustrated in Figs 9 and 10. Figure 9 shows the yield from a molybdenum target with and without a

cesium film. Figure 10 shows the same type of data for a stainless steel target. There is certainly no large effect due to the cesium.

### CONCLUSIONS

A simulated micrometeorite impact into a solid target serves to concentrate the particle energy into a small volume. This large energy per unit volume results in a high local temperature. The high temperature creates a small ball of gas and a dilute plasma of ions and electrons which expand out away from the impact site.

Variation of target temperature up to 600°C does not affect the amount of charge produced. Neither will an applied electric field, since it is not an emission phenomenon. The presence of thin surface layer contaminants does not materially affect the charge yield. Target material is an important parameter in a way which is not understood. However, refractory metals produce a higher charge yield than materials such as copper or stainless steel.

## II. DISCHARGES IN ION ENGINES

Discharges have been initiated in simulated ion engines by particle impacts. It has proved surprisingly easy. The first attempts were made in a clean system, with no cesium. The experimental arrangement had a tantalum plate for a target and a copper plate acting as a grid. The copper plate was located 1.0 mm away from the target. Particles from the accelerator passed through an 0.8-mm hole in the copper plate and impacted on the tantalum target.

With a voltage of 6000 volts applied between target (-) and grid (+), approximately 5% of the impacts were observed to produce discharges. The threshold voltage was approximately 5000 to 6000 volts. It was easier to produce discharges with the grid positive, with respect to the target, than with a negative grid. However, some discharges were observed with the grid negative although the frequency of occurrence was approximately a factor of ten lower. The effect of the voltage polarity is discussed more fully below.

Following these preliminary observations, breakdowns in the presence of cesium were observed. The experimental

arrangement used was the one used for charge yield measurements. The target was tantalum, the tungsten grid was located 3.5 mm away and the grid had a transmission of approximately 90%. In the presence of cesium, impact-initiated discharges commenced when the applied voltage was approximately 3500 volts. The percentage of impacts producing discharges was about double the case with no cesium.

Illustrated in Fig. 11 are tracings of typical oscilloscope pictures taken, which demonstrate that it is really the particle which causes the discharge. Figure 11-a shows a particle which does not cause a discharge. The upper trace is of the particle detector, vertical sensitivity 0.2 volt/div and sweep speed 10  $\mu$ sec/div. The lower trace was made with a Tektronix Model P-6013 high voltage probe connected to the grid where the high voltage is applied. The oscilloscope gain and probe attenuation are such that the vertical sensitivity is 2000 volts/div. The probe trace is triggered automatically by the top trace and also has a sweep speed of 10  $\mu$ sec/div. A positive voltage of 3500 volts was applied to the grid, while the target was grounded through a one-ohm resistor.

In Fig. 11-a, a particle is observed to pass through the detector in about 12 microseconds. It impacts on the target about 22 microseconds after leaving the detector. At this time some of the charge released by the impact is observed in the detector signal. There is no change in the grid voltage, as shown by the straight lower trace.

Figure 11-b illustrates a particle which causes a discharge. The high voltage, vertical sensitivities and sweep speeds are the same as in Fig. 11-a. The particle passes through the detector in about 15 microseconds and impacts on the target about 28 microseconds later. At this time a discharge occurs, evidenced by the abrupt change of about 2800 volts in the grid voltage. The detector trace disappears off scale as the sensitive amplifier picks up the signal from the discharge.

Many such discharges have been observed, always caused by particles. If particles do not bombard the surface, but the experiments simply stands with the high voltage applied, there are no discharges. This fact indicates that the system is safely below the point of natural breakdown.

The discharge behavior as the available energy is varied has been observed by changing the capacitance in parallel with

the grid. Figure 12 illustrates the high voltage on the grid during the discharge with three different capacitances. The oscilloscope tracings in Fig. 12 show the grid voltage as measured by the high voltage probe. Vertical sensitivity is 2000 volts/div, sweep speed is 0.2  $\mu\text{sec}/\text{div}$ . Figure 12-a had only the probe capacitance of  $\sim \mu\text{f}$  in parallel with the grid. Figure 12-b had a capacitance of 500  $\mu\text{f}$  and 12-c, a capacitance of 0.06  $\mu\text{f}$ .

The discharge times are all comparable. The different shapes of the curves, particularly 12-a, are not, as yet, understood. The times are long enough so that the frequency response of the probe is not a factor in determining the shape of the curves.

A qualitative description of the discharge may be given from visual observations. With +3500 volts on the grid and a capacitance of 500  $\mu\text{f}$  in parallel with the grid, the discharge is barely visible, appearing as a tiny pinpoint of light very near the target surface, presumably close to where the particle impacts. If the capacitance is raised to 0.002  $\mu\text{f}$ , more light is emitted, concentrated in two regions. There is a luminous blue glow on the surface of the target, a dark space between target and grid, and then a luminous blue glow around the grid.

Photographs of some discharges are reproduced in Fig. 13. They were made by keeping the lens of a Polaroid camera open throughout the time of discharge, so that each picture is of the total integrated light output. Figure 13-a, taken in normal light, illustrates the field of view. Particles enter from the right, pass through the four element detector and then through the grid and impinge on the target.

The grid is a 3/8" hole in a solid plate, covered with tungsten mesh. In the picture it appears as a solid plate just to the left of the last detector tube. The target appears as a thin line just to the left of the grid. Grid-to-target spacing is 3.5 mm.

Figure 13-b is a photograph of a discharge with a grid capacitance of 0.002  $\mu\text{f}$  and +3500 volts applied to the grid. In Fig. 13-c the capacitance and voltage are the same but the applied voltage is negative. In Figs. 13-d and 13-e the grid capacitance is 0.06  $\mu\text{f}$  and the grid voltage is 3500 volts, positive in Fig. 13-d and negative in 13-e.

There is a noticeable difference in both sets of photographs between grid positive and grid negative. With a

positive grid, the discharge appears to spread from an impact point on the target out to the grid. Observed discharges with a negative grid always appear to spread from an impact on the grid forward to the target and backward to the detector elements.

These pictures are interpreted to mean that discharges have really been observed only when the impacting point is negative with respect to its surroundings. This would account for the decreased frequency of grid-negative discharges noted before. In any given experiment many more particles strike the target than the grid.

The discharges have also been photographed with an STL Fast Camera. This camera will take three frames separated by as little as 0.5  $\mu$ sec, with exposure times of 5 to 200 nanoseconds. It can also be used as a streaking camera, with the streak-time variable from several nanoseconds to several microseconds.

An example of the framing pictures taken is shown in Fig. 14. Figure 14-a is an oscilloscope tracing showing the exposure times and synchronization of the exposures relative to the discharge voltage. The rectangular pulses in the top trace are the three exposures of the camera. The bottom trace represents the high voltage to the grid, with a vertical scale of 2000 volts/div. The two sweeps are triggered together and are sweeping at a rate of 0.5  $\mu$ sec/div. Thus the first exposure occurs while the capacitor is discharging and the other two somewhat later.

The grid capacitance was 0.06  $\mu$ f and the applied voltage was 3500 volts. The cesium gun was spraying cesium at the target, and the grid-to-target spacing was 3.5 mm. The image is magnified and the target is the flat plate at the bottom of each frame while the grid is directly opposite. In some frames luminous material can be seen moving through the grid (the grid is a 3/8"-diameter hole in a flat plate).

Two separate discharge photographs are reproduced in Fig. 14-b, and in each case the first frame is the one on the right. Perhaps the most obvious conclusion to be drawn is that material appears to erupt from the target and is roughly symmetrical about the point where the particle impacts. It is apparent that energy delivered to the grid is spread out over a much larger area than is the case on the target. At least during the time that the grid voltage is falling there is only a small luminous spot in the vicinity of the target; presumably most of the current is going into this spot.

Figure 15 is a reproduction of two streak pictures. The oscilloscope tracing in 15-a illustrates the length of the streak and the time relationships. The top trace shows the duration of the streak and the second trace shows the high voltage on the grid. As before, the vertical scale on the grid voltage trace is 2000 volts/div and the sweep speed on both traces is 0.5  $\mu$ sec/div.

Two streak photographs are reproduced in Fig. 15-b. The duration of the streak is 2  $\mu$ secs. There was no slit in the system and the whole image, as shown in Fig. 14-b, is being moved across the film. The streak starts at the right and moves to the left. A small luminous spot on the target can be seen during the first part of the streak. This spot then seems to disappear and still later more luminous material starts to move out from the target. There are still a large number of points about these discharges which are not understood.

### CONCLUSIONS

The impact of a micrometeorite can initiate a discharge in a simulated ion engine. The voltages, spacings and materials in the simulated engines are all in the range of operating engines. All the discharges observed so far, have apparently occurred when the impact point is negative with respect to its surroundings. The mechanism by which the discharge is initiated is not understood, but it is believed that the neutral material ejected from the impact site is an important factor.

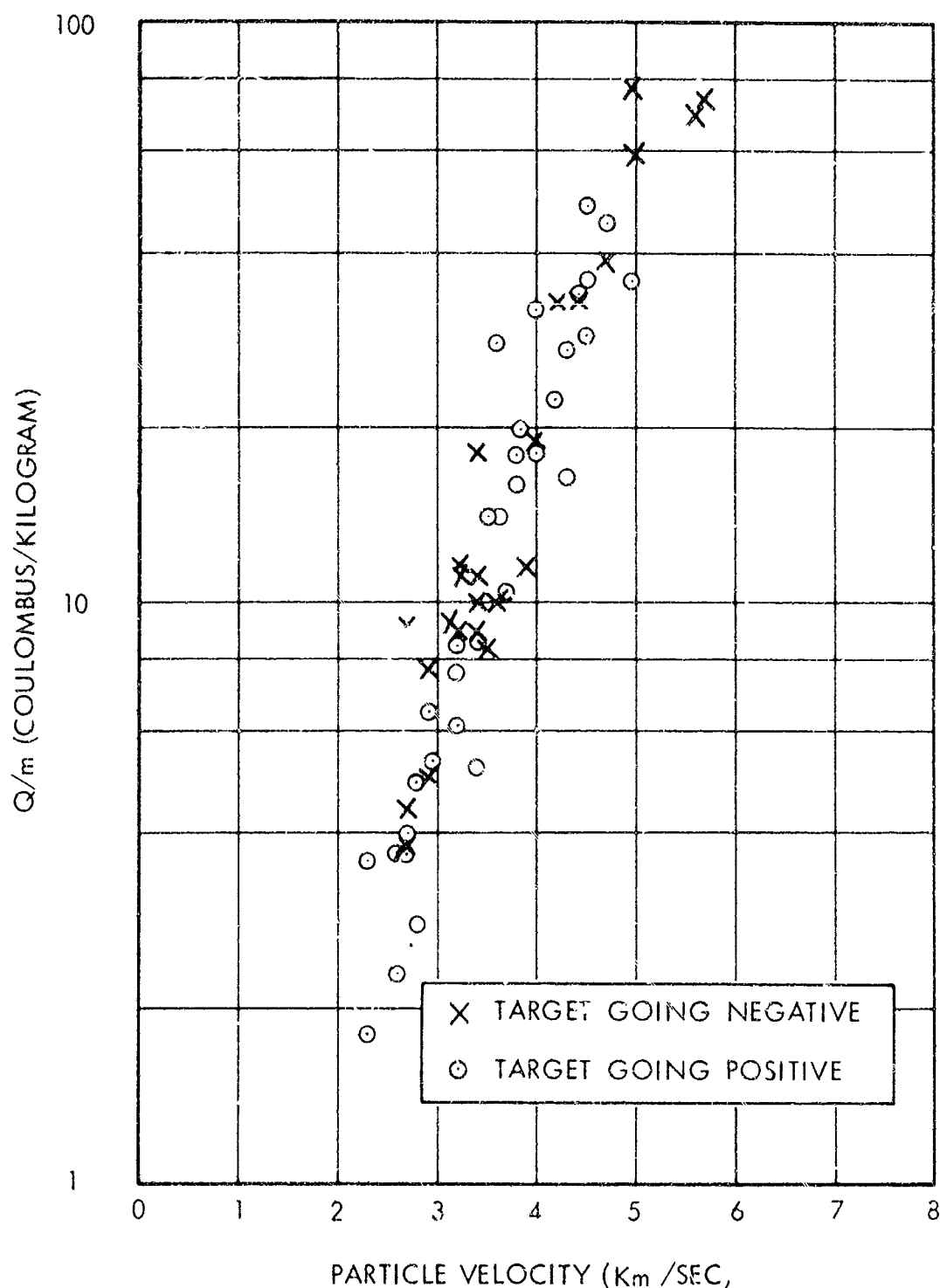


Figure 1. Data illustrating the equality of positive and negative charge emission. The target was tungsten. The emitted charge, normalized to the mass of the impacting particle, is plotted as a function of particle velocity. The particles were iron spheres, ranging in diameter from 0.1 micron to 1.0 microns.

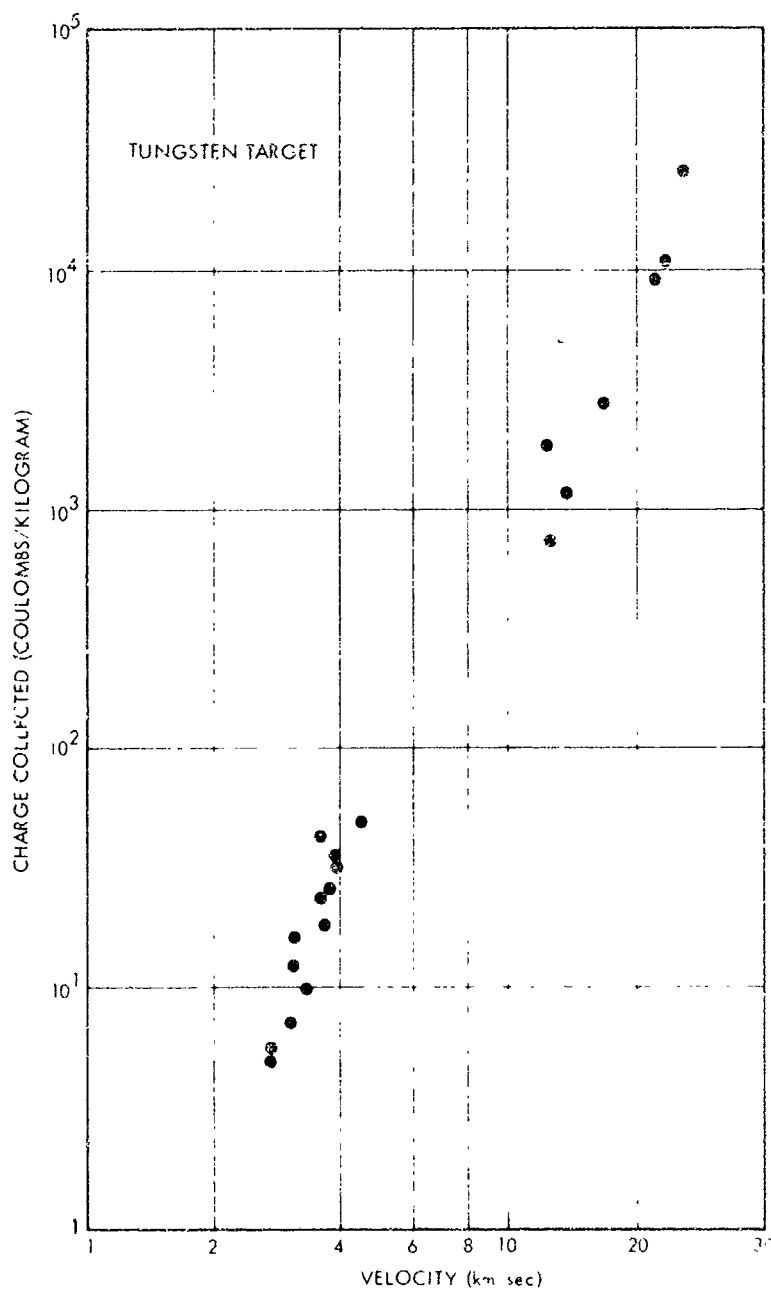


Figure 2. Charge emission from a tungsten target. Emitted charge, normalized to the impacting particle mass, is plotted against the particle velocity. The particles were iron spheres, ranging in diameter from 0.1 micron to 1.0 micron.

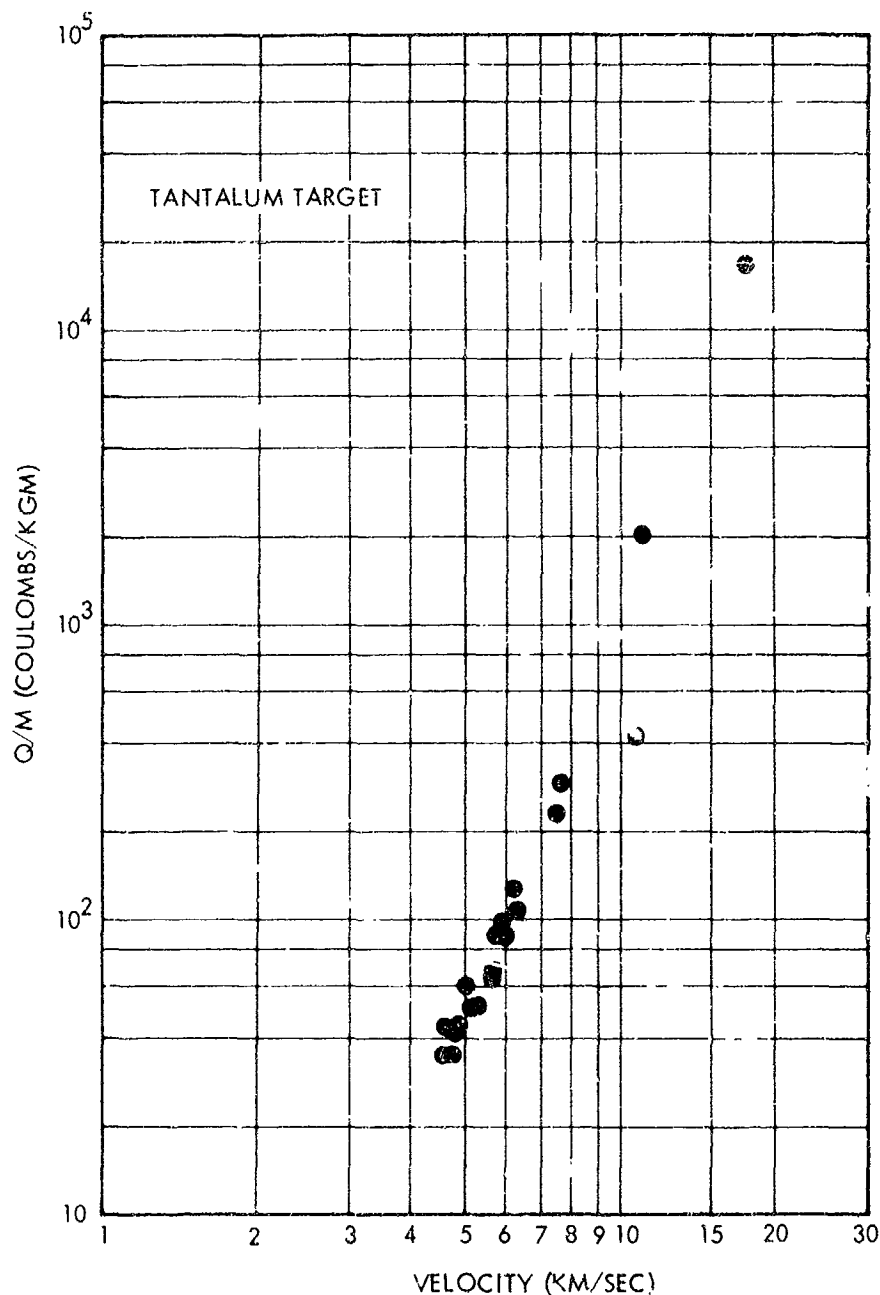


Figure 3. Charge emission from a tantalum target. Emitted charge, normalized to the impacting particle mass, is plotted against the particle velocity. The particles were iron spheres, ranging in diameter from 0.1 micron to 1.0 micron.

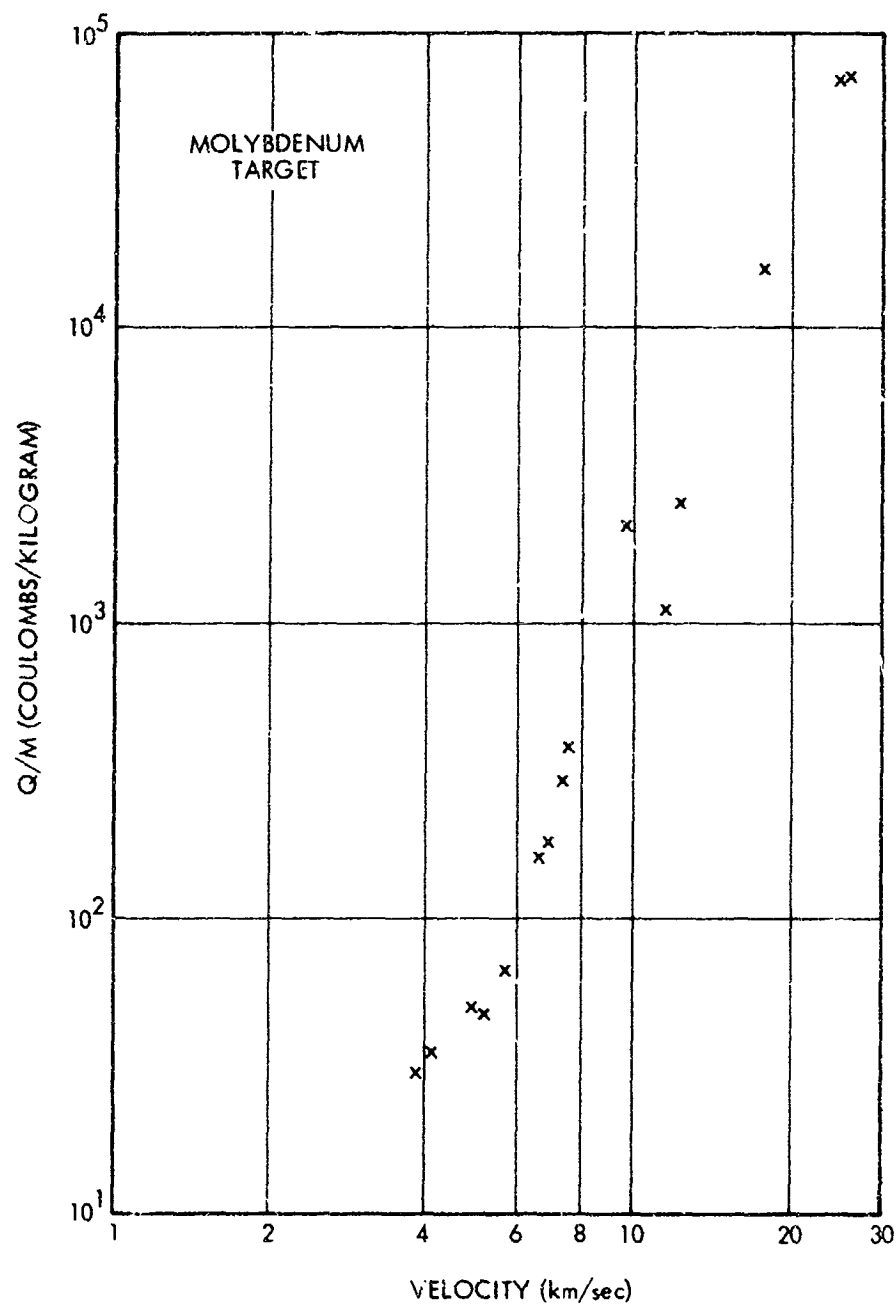


Figure 4. Charge emission from a molybdenum target. Emitted charge, normalized to the impacting particle mass, is plotted against the particle velocity. The particles were iron spheres, ranging in diameter from 0.1 micron to 1.0 micron.

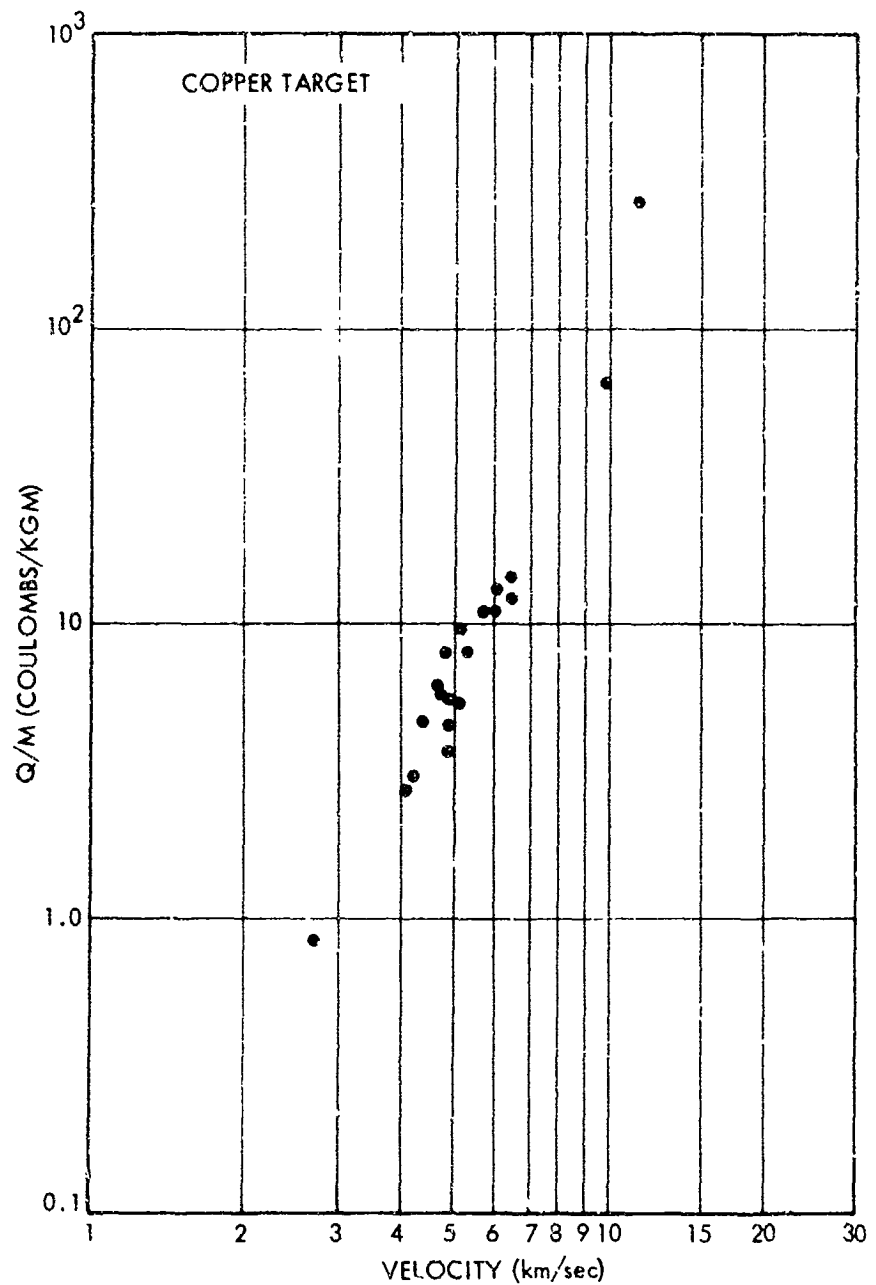


Figure 5. Charge emission from a copper target. Emitted charge, normalized to the impacting particle mass, is plotted against the particle velocity. The particles were iron spheres, ranging in diameter from 0.1 micron to 1.0 micron.

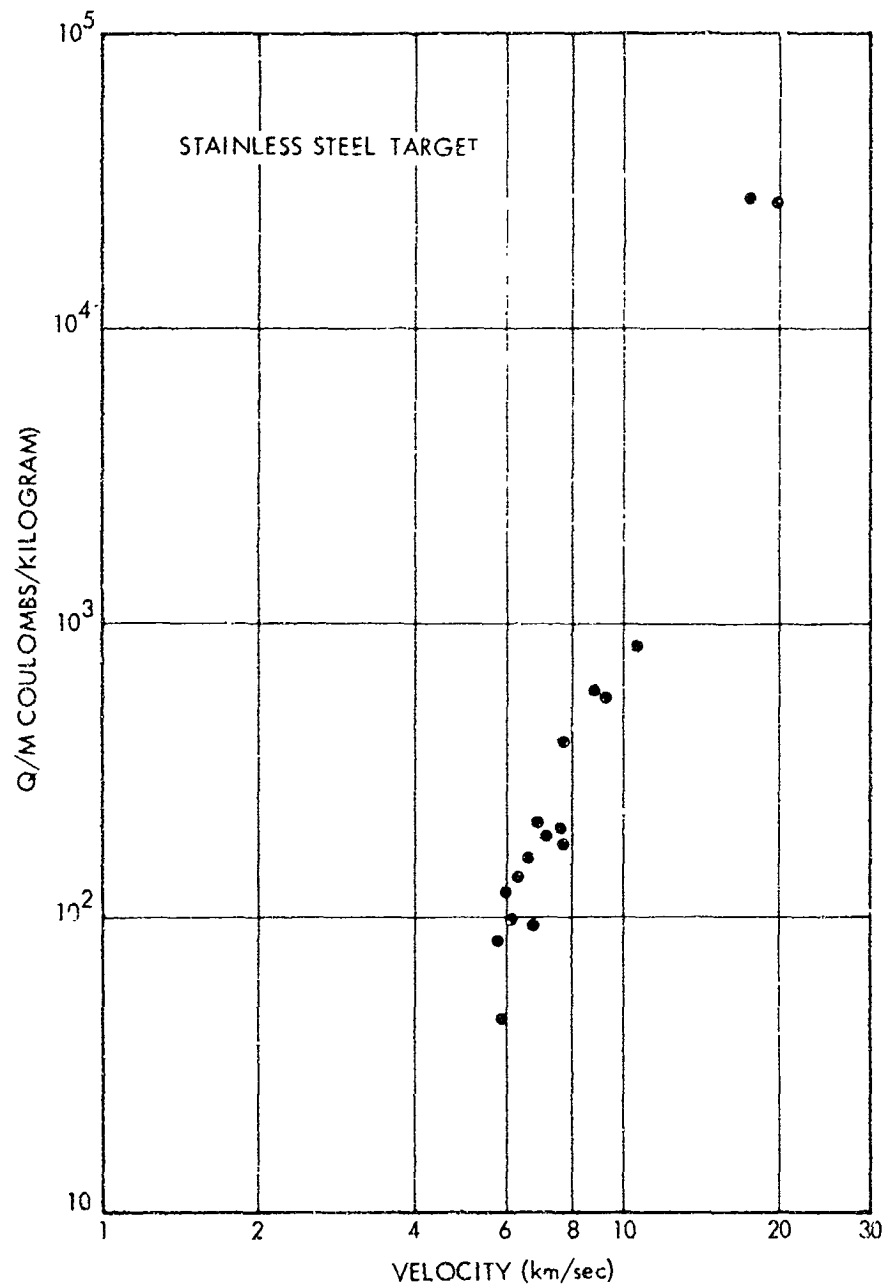


Figure 6. Charge emission from a stainless steel target. Emitted charge, normalized to the impacting particle mass, is plotted against the particle velocity. The particles were iron spheres, ranging in diameter from 0.1 micron to 1.0 micr

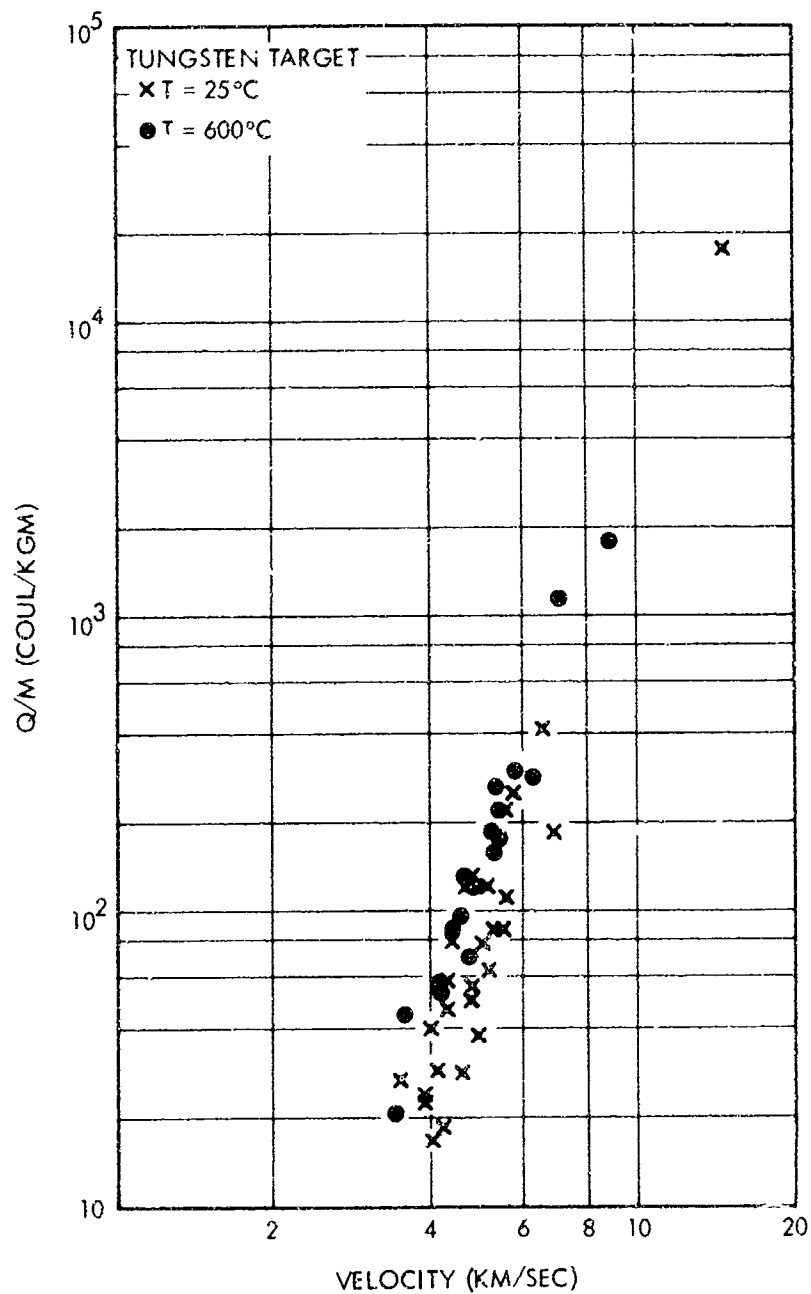


Figure 7. Charge collection from a tungsten target at target temperatures of  $25^\circ\text{C}$  and  $600^\circ\text{C}$ . The ordinate is emitted ch normalized to the impacting particle mass and the abscissa particle velocity. The particles were iron spheres, ranging in diameter from 0.1 micron to 1.0 micron.

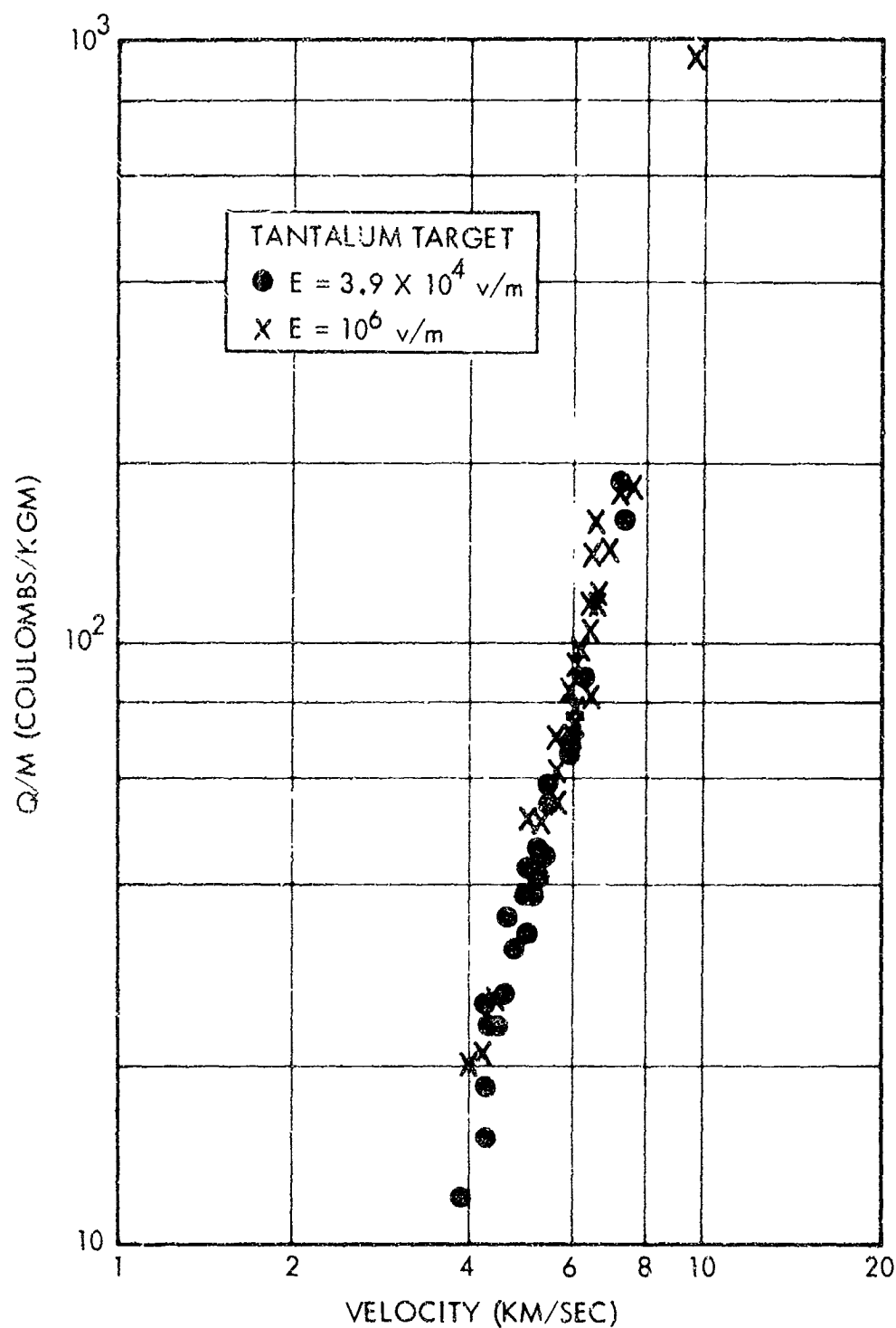


Figure 8. Effect of electric field on charge emission from tantalum target. The emitted charge, normalized to the impacting particle mass, is plotted against particle velocity. The particles were iron spheres, ranging in diameter from 0.1 micron to 1.0 micron.

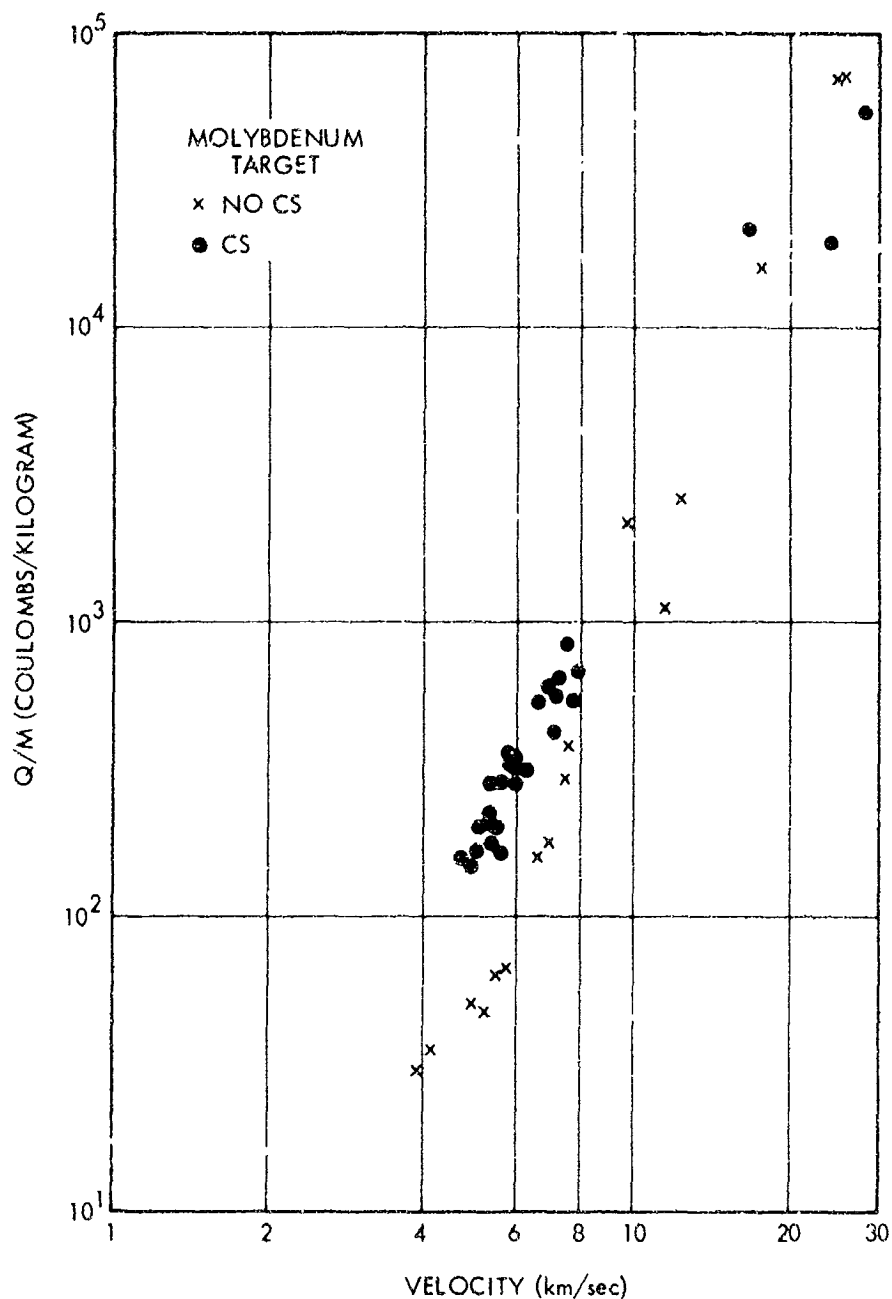


Figure 9. Charge emission from a molybdenum target showing the effect of a thin cesium film on target surface. The emitted charge, normalized to the impacting particle mass, is plotted against particle velocity. The particles were iron spheres, ranging in diameter from 0.1 micron to 1.0 micron. The estimated Cs coverage was a layer 0.1 micron thick.

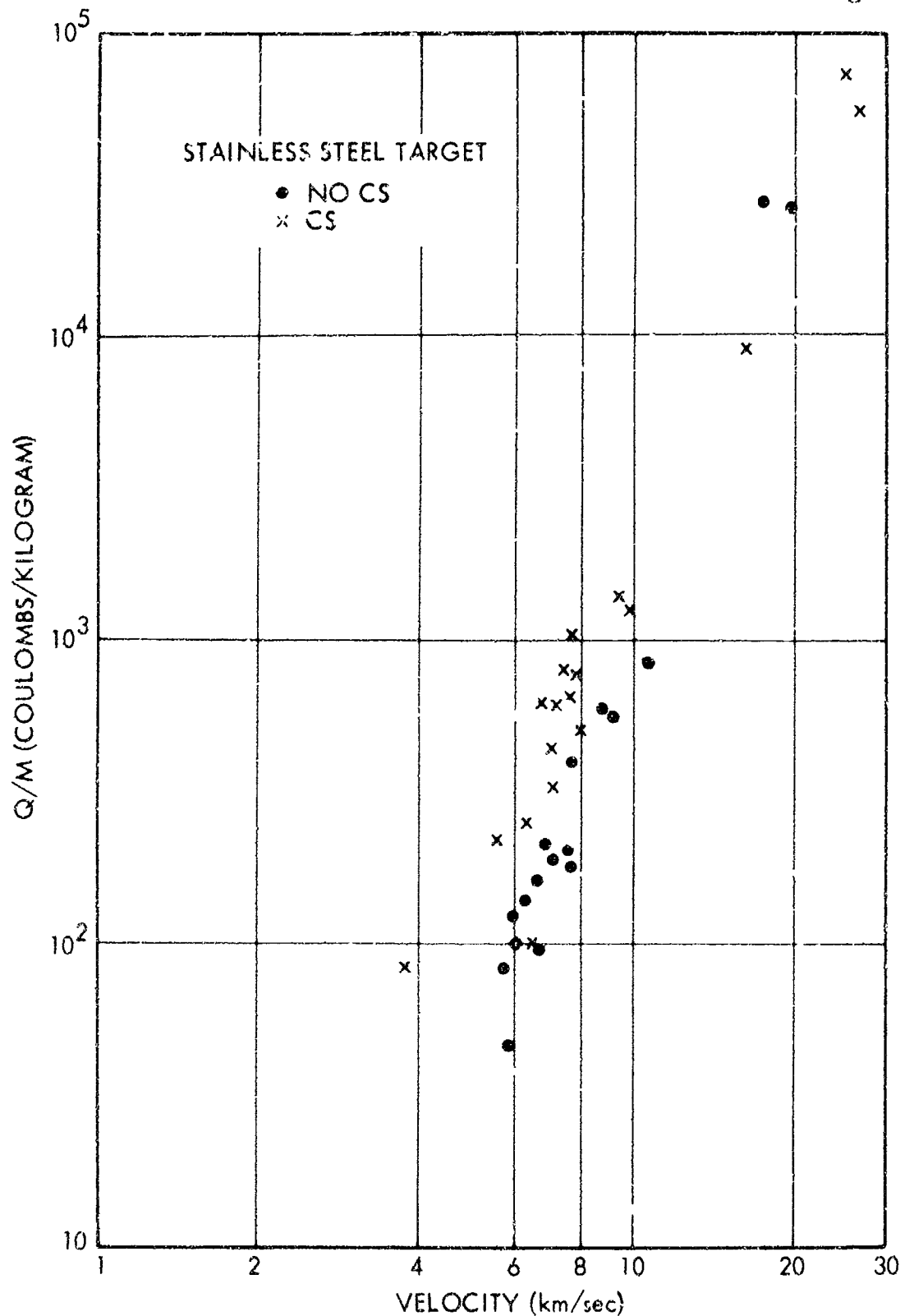


Figure 10. Charge emission from a stainless steel target showing the effect of a thin cesium film on target surface. The emitted charge, normalized to the impacting particle mass is plotted against particle velocity. The particles were iron spheres, ranging in diameter from 0.1 micron to 1.0 micron. The estimated Cs coverage was a layer 0.1 micron thick.

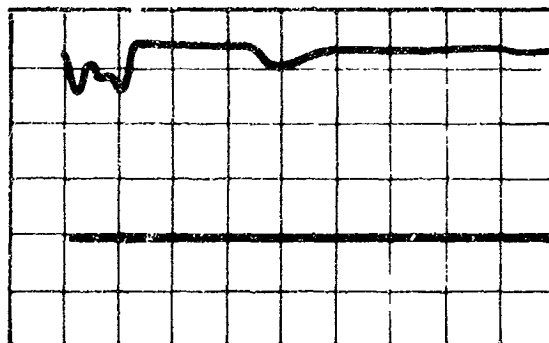


Figure 11-a  
(No Discharge)

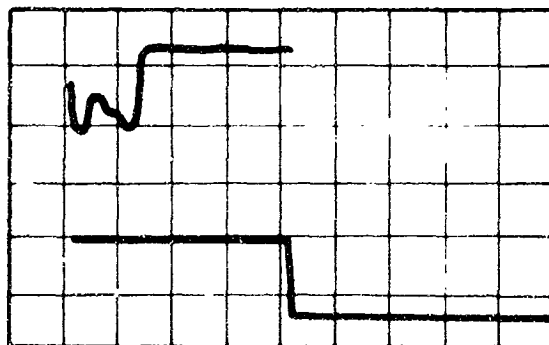


Figure 11-b  
(Discharge)

Figure 11. Oscilloscope tracings illustrating a particle which does not cause a discharge (11-a) and one which does (11-b). In both figures the top trace is of the particle detector, vertical sensitivity 0.2 v/div and sweep speed 10  $\mu$ sec/div. The bottom trace is from a high voltage probe connected to grid in front of the target, vertical sensitivity 2000 volt/div and sweep speed 10  $\mu$ sec/div.

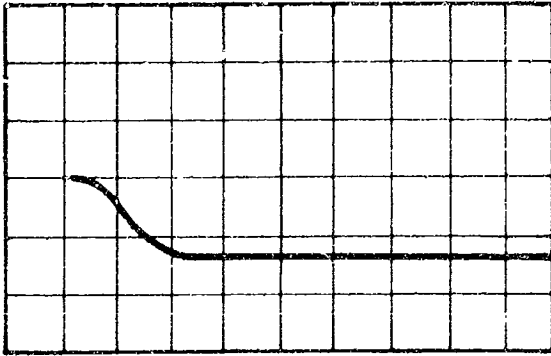


Figure 12-a

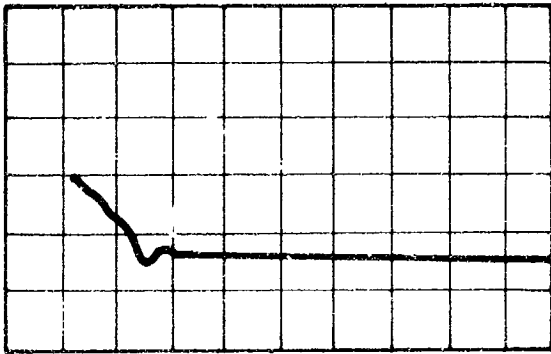


Figure 12-b

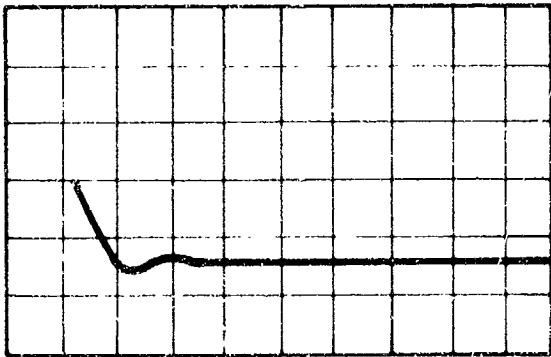


Figure 12-c

Figure 12. Behavior of the high voltage on the grid during discharge with three different capacitors in parallel with the grid. Vertical scale is 2000 volts/div. sweep speed is 0.2  $\mu\text{sec/div}$ . Capacitances are: (12-a)  $C = \mu\text{f}$ , (12-b)  $C = 500 \mu\text{f}$  (12-c)  $C = 0.06 \mu\text{f}$

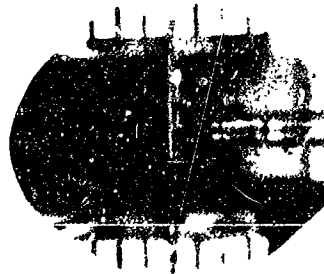


Figure 13-a

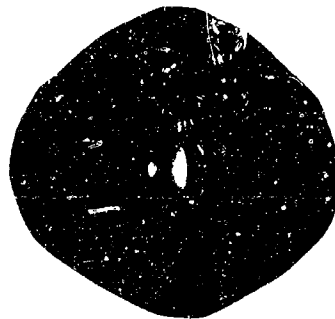


Figure 13-b

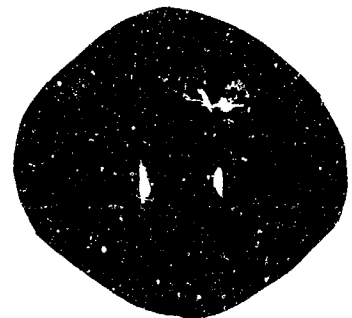


Figure 13-c

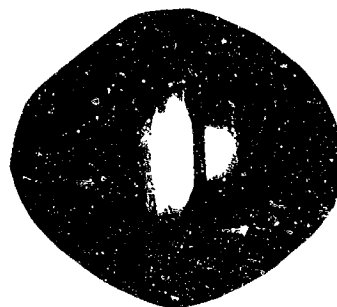


Figure 13-d

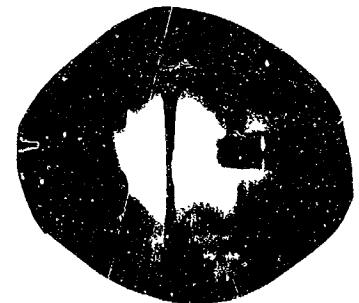


Figure 13-e

Figure 13. Polaroid pictures of particle initiated discharge. Figure 13-a shows the field of view, with a particle detector on the right, the grid just to the left of the particle detector and then the target to the left of the grid. The target appears as a thin line in the photograph. Figures 13-b and 13-d are with a positive voltage applied to the grid and 13-c and 13-e with a negative voltage. See text for a full discussion.

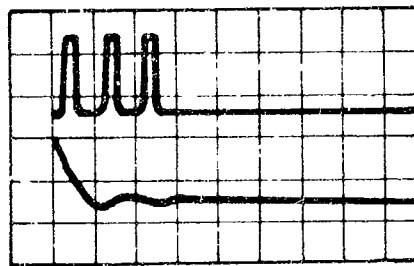


Figure 14-a

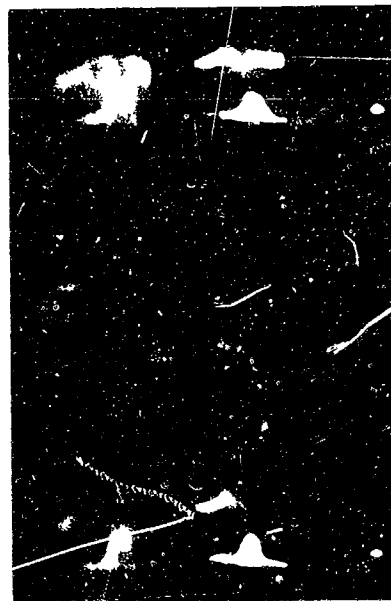


Figure 14-b

Figure 14. Fast-camera framing pictures of particle initiated discharges. The oscilloscope tracings show the time relationship between the three exposures (top trace) and the discharging high voltage on the (bottom trace). The sweep speeds were both  $0.5 \mu\text{sec/div}$ . Two separate discharges are shown in the photograph and the exposure on the right is the first in both cases.

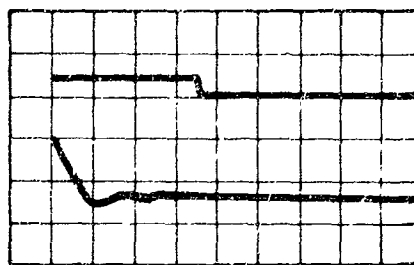


Figure 15-b

Figure 15. Fast-camera streak pictures of particle initiation discharges. The oscilloscope tracings show the time relationship between the streak time (top trace) and the discharge high voltage on the grid (bottom trace). The oscilloscope speeds are both  $0.5 \mu\text{sec}/\text{div}$ . There was no slit in the system and the entire image (as shown in Fig. 14) is being swept across the film. Two discharges are shown and in both cases the sweep starts at the right and moves to the left.